Cross Calibration Report of the EDI Measurements in the Cluster Active Archive (CAA)

prepared by

E. Georgescu, P. Puhl-Quinn, H. Vaith, H. Matsui

maintained by

M. Rashev

Table of content

1 Introduction

EDI is designed to measure the electron drift velocity and the 2D electric field $\mathbf{E}_{\perp}$ perpendicular to the ambient magnetic field **B**, when the gradient of **B** in the plane perpendicular to it can be neglected. As a by-product it measures the total magnetic field at high time resolution (sampled at few 10 msec resolution).

When the guns do not emit electrons the detectors can be used to measure ambient electron counts in a narrow energy range of 0.5keV or 1keV. These measurements are available in both active and passive mode. In active mode(electric field mode, also known as windshield wiper mode) the ambient electro counts are sampled whenever the emitted electron beams do not return to the spacecraft. These data are available in the QZC dataset. In passive mode(ambient electron mode) the ambient electron counts are available in AE and AEDC datasets.

Therefore EDI provides four types of measurements that need to be calibrate and can be compared with other measurements:

- Electron drift velocity
- DC electric field
- Total magnetic field
- Flux of 1 keV (or sometimes 0.5 keV) electrons

2 Instrument Description[1]

The EDI instrument and its modes of operation are described in detail in the ICD [1], Paschmann et al. [2], Quinn et al. [3], available online at the CAA site, and Paschmann et al [8].

The basis of the electron-drift technique is the injection of weak beams of electrons perpendicularly to the ambient magnetic field and their detection after one or more gyrations. In the presence of a drift velocity, the circular electron orbits are distorted into cycloids. Their shape depends on whether the beam is injected with a component parallel or anti-parallel to the drift velocity. The lengths of the two orbits and the electron travel times differ. To be able to realize both types of orbits simultaneously, EDI uses two guns and two detectors.

The instrument records firing directions of the guns and the times of flight of the electrons. The magnetic field information is received through the inter-experimental link from the FGM (flux-gate magnetometer) in order to be able to send electrons perpendicular to the magnetic field vector. The final data products contain the electron drift velocities and the perpendicular electric field in Cartesian GSE coordinate system (corrected for spacecraft motion).

This active operation mode is called **W**indshield **W**iper (“WW”) because the beams are swept quickly back and forth until detection is achieved or **Electric Field** (EF) mode.

EDI also operates in a passive mode, whereby **Ambient Electron**s are detected (AE-mode). The guns are not operating in this case and the detectors record the ambient electron counts for a fixed time interval (1/64, 1/128 seconds) with high sensitivity and time resolution (16 or 128 samples/s), at fixed energies (0.5 or 1 keV) and pitch angles (0°, 90°, 180°). Counts are accumulated synchronously by the two detectors and each counts pair is stored in telemetry with its

corresponding look direction, expressed in spinning spacecraft coordinates (azimuth and polar angle). The AE product in the CAA contains the look direction of the detectors in GSE as well.

3 Measurement Calibration Procedures

3.1 Drift velocity/Electric field measurements

The measurement principle is relatively straightforward in that it does not depend on any time dependent factors such as offsets, scaling or aging effects. The measured quantities are time differences (time-of-flight) and direction. The electron beam direction is determined by electric voltages applied in a complex geometry; the conversion table, voltages to angles, has been determined prior launch and is part of the onboard software of the instrument.

3.2 Ambient electron measurements

The ambient electron rates are recorded for fixed pitch angles in the AE-mode, as mentioned in section 2. In order to obtain a useful physical quantity, directional flux for instance, one must apply some corrections and make a calibration relative to the PEACE instrument. Otherwise the raw electron count rates can be used for plasma boundary detection.

The complete procedure of AE correction and calibration contains 3 steps:

1. Intra-detector correction for the detector look direction by using the AEC files
2. Inter-detector correction
3. Calibration relative to PEACE

More details of these steps are explained in sections 5 and 6.

4 Measurement Processing Procedures

The processing procedures of the EDI data are described in the ICD [1]. Post-processing of EDI data in view of comparison with other instruments are imposed by the statistic nature of the EDI measurements and by the high but irregular resolution of the time series. Two post-processing procedures have been used: (1) averaging and (2) interpolation.[2]

Most frequently averaging to the regularly spaced time intervals of the lower resolution measurements of the other instruments is used. This helps also to reduce the statistical spread of the data points.

For the comparison with the high resolution, smooth FGM measurements, the FGM data were interpolated to the EDI beam times.[3]

The post-processing of data for each cross-calibration activity is mentioned in the corresponding subsection of Section 6.

5 Results of Calibration Activities

Calibration of the EDI instrument was done pre-flight in order to determine the dependence of the beam directions on the applied voltages. These calibration tables are part of the on-board software and were not changed during the mission. [4]

The intra-detector and inter-detector corrections performed in the "AE" mode as described in Section 6.4 can be considered pre-calibration activities.

5.1 Drift velocity/Electric field measurements

As explained in section 3, these measurements being fundamentally time-of-flight and recorded voltages of beams that returned to the spacecraft and were registered by the detectors are not influenced by the spacecraft and by time dependent factors, so they do not have in-flight calibration issues.

5.2 Ambient electron measurements

5.2.1 Intra-detector correction for the detector look direction by using AEC files

The AE files in the CAA contain time series of electron counts for both detectors and the three possible pitch angles, the status-byte, specifying the detected energy and the telemetry mode and the look direction for Detector 1 in spherical polar instrument coordinates (theta, phi) and in Cartesian GSE coordinates. AEC files contain correction factors for 139 spherical polar(theta) angles for both detectors (**f1_D1**, **f1_D2**) and for 128 azimuthal(phi) angles for both detectors (**f2_D1**, **f2_D2**). Each **raw_count** must be corrected by the factors corresponding to **theta, phi:**

corrected_count1 = raw_count*f1(thetat)*f2(phi)/(2. – tm)

where **f1(phi), f2(theta)** from AEC files**, tm = 0,1** for 16/128 Hz sampling rate **(tm = status/2)**.

This correction is now done at CAA and a new product is available for the user containing corrected ambient electron counts. The product is called C#_CP_EDI_AEDC__yyyymmdd_Vvv.cef

5.2.2 Inter-detector correction

As seen in Figure 5.1 after correcting for the look direction there is a clear discrepancy between the **corrected_count1** from the two detectors. We need the inter-detector correction factors (**f_id**) to correct for this:

corrected_count2 = corrected_count1*f_id

where **f_id** = D1/D2, and D1 and D2 are averages of look direction corrected raw data counts, that is, D1=< **corrected_count1_D1>** and D2=< **corrected_count1_D2>**.

In Figure 5.2 we show an example of inter-detectors correction. The averages were made in this case over the whole time interval. The **f_id** vary in time and the problem is to select appropriate time intervals for the averaging. There are plans that the EDI team provide files with inter-detector correction factors.

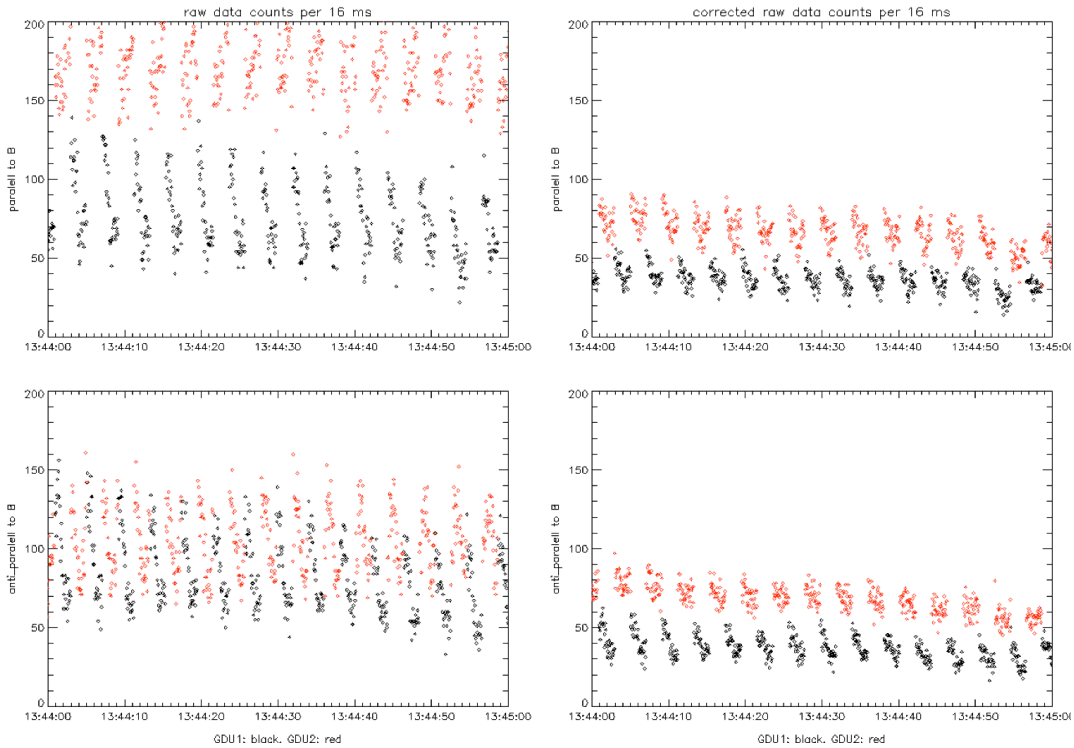

Figure 5.1. Ambient electron counts with pitch angle 0° (upper panels) and 180° (lower panels) during one minute of measurements. **Raw_counts** are on the left, **corrected_count1** on the right. The colors distinguish between the 2 detectors: GDU1 - black and GDU2 - red. The alternating colors in time (every half spin) show the switching of look directions.

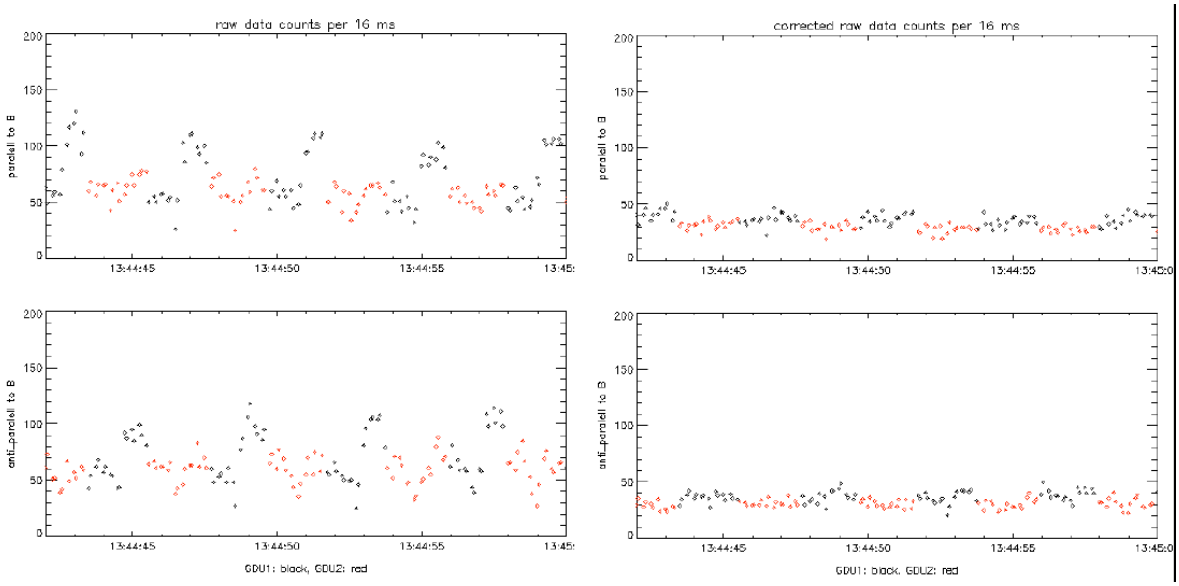

Figure 5.2. Inter-detector correction for **corrected_count1** with pitch angle 0° (upper panels) and 180° lower panels. **corrected_count1** on the right **corrected_count2** on the left. GDU1: black and GDU2: red.

5.2.3 Statistics on inter-detector and inter-spacecraft comparison

In order to study the long term evolution of the inter-detector efficiencies, averages of omni-directional corrected_count1, i.e. AEDC data, for each detector and spacecraft have been computed on hourly respectively daily basis. Three months (February to April) for four years (2005-2008) have been used, because then the spacecraft spent longer time in the solar wind where similar fluxes are expected to hit all detectors.

The comparison was done between detectors on the same spacecraft and on different spacecraft. Figure 5.3 shows the daily inter-detector ratios for C1, C2, and C3 (i.e. three months from each year joint together). The jump on Feb. 17, 2007 in the C1 data is due to MCP voltage change for detector 1, all the other changes have unknown reasons. Table 1 summarizes all MCP voltage changes for the EDI detector units from the beginning of the mission till April 2017. There is only one further change possible on detector 2 on C1.

The comparison of hourly averages of the ratios of omni-directional counts is shown in Fig. 5.4. The top panel shows the inter-detector ratios for the 3 spacecraft, similarly to Fig. 5.3 only with a larger spread in the data, since the inter-detector factors change on a smaller scale than one day.

The comparison between detectors of different spacecraft is shown on the bottom panel of Fig. 5.4. Measurements of detector 1 on C2 and C3 were compared to detector 1 on C1.

	C1		C2		C3	
Time	D1	D2	D1	D2	D1	D2
2001-01-09T15:28	2	2	4	4	3	3
2002-11-16T07:29					4	
2003-02-28T20:20	3	3				
2003-04-19T23:14			5			
2003-05-11T09:07				5		
2004-02-09T00:20			6			4
2004-03-06T00:42	4	4			5	
2005-09-11T18:48	5					
2005-09-12T17:00					6	
2005-10-22T02:07		5				5
2006-11-11T11:54			7	6		
2007-02-17T02:25	6				7	6
2017-02-13T03:15						7
2017-04-17T09:19	7	6		7		

Table 1. EDI MCP voltage changes. A number marks the detector and voltage range for which the voltages have been raised.[5]

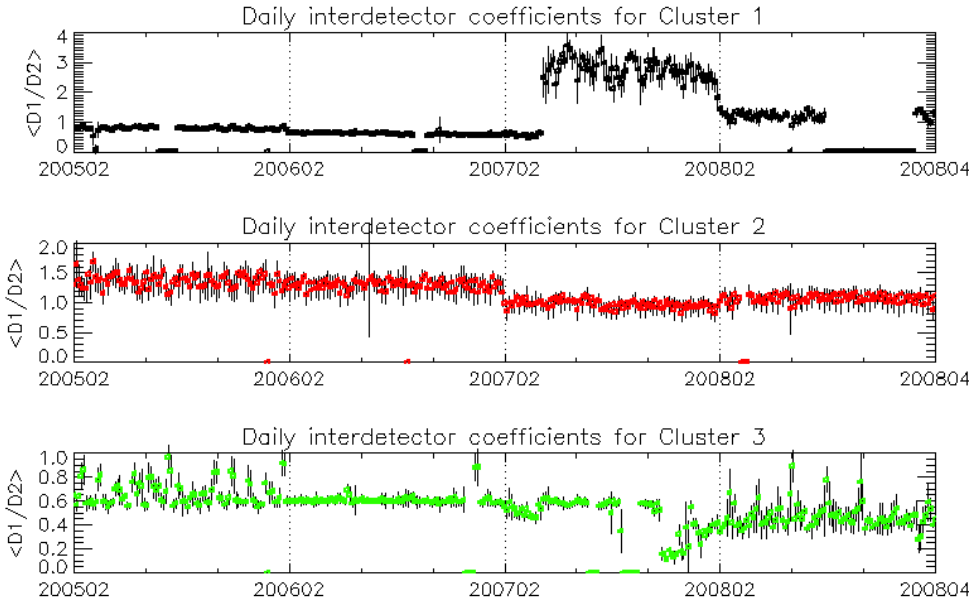

Figure 5.3 Mean daily inter-detector coefficients, obtained by averaging the ratios of omni-directional counts for detector 1 and detector 2 on the same spacecraft. The error bars show the standard deviation. The interval between subsequent year-ticks contains 3 intervals corresponding to the months: February-April

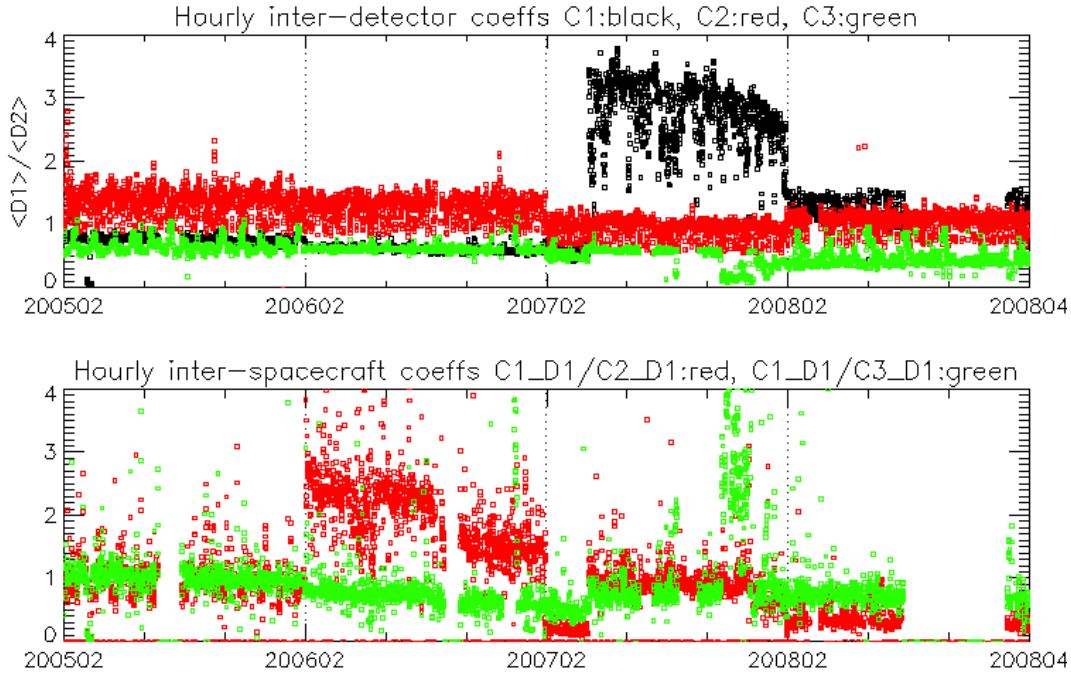

Figure 5.4 Ratios of hourly averages of omni-directional flux ratios for the 3 s/c. Top panel: inter-detector comparison, bottom panel: inter-spacecraft comparison. Detector 1 measurement have been compared for different spacecraft

6 Results of Cross-Calibration Activities

The cross-comparison activities supported by the EDI team are:

- Compare the magnetic field magnitude resulting from the electron time-of-flight measurements (EGD) with FGM and WHISPER data
- Compare drift velocity and electric field measurements to the corresponding measurements by EFW, CIS and PEACE experiments
- Compare ambient electron count rates to PEACE

6.1 EDI and FGM comparison

In calibration of the FGM instrument EDI time-of-flight data were used from the beginning of the mission to check the FGM calibration and to determine the spin axis offset for the daily calibration files. The obtained accuracy was up to 0.3 nT for fields below 1000 nT, with the possibility to reduce it below 0.1 nT by using special calibration files (Georgescu E. et al [4]).

Since the beginning of the archiving activities the FGM team started to produce high-resolution FGM data with different calibration files than the daily ones. A systematic comparison of the CAA data with the EDI data was performed for a list of selected dates.

The results presented in form of histograms of ratios and differences of the magnetic field magnitude determined by the two instruments, showed a systematic asymmetry in the histogram of the differences and a shift of the ratios around 0.3% (Figure 6.1).

The following table summarizes the results of the comparison for the selected orbits for 2002 for the three spacecraft. First line for each spacecraft is for daily calibration second with CAA data.

Year	S/C	<Bedi/Bfgm>	stddev	<Bedi-Bfgm, nT>	stddev, nT
2002	1	100.45	0.28	1.23	0.81
		100.36	0.30	1.00	0.91
	2	100.29	0.35	0.90	1.06
		100.28	0.30	0.86	0.93
	3	100.26	0.29	0.86	0.99
		100.38	0.29	1.11	0.94

Table 2. Comparison of magnetic field magnitude from FGM and EDI.

Since EDI has no regularly spaced time series, following method was used to match them:

- EDI: all measurement points were used
- FGM: 1 s averages, produced with the daily and with CAA calibration files, were interpolated to EDI times

No distinction was made here for the different FGM ranges. Data are in the ranges:

3 -256 nT < B < +255.97 nT, digital resolution 0.03125 nT and
4 -1024 nT < B < +1023.9 nT, digital resolution 0.125 nT.

Separations of the data by FGM ranges were tried, but they didn't show a different behavior of the ratios. No significant differences were observed between the FGM data calibrated with the daily calibration files (used for the production of CSDS prime parameters) and those from CAA.

Further studies using a more extended data base found however a discrepancy between the field magnitudes in the CAA and those calibrated with the daily calibration files of up to 1% (see the EDI-FGM multispacecraft comparison plots on CAA)

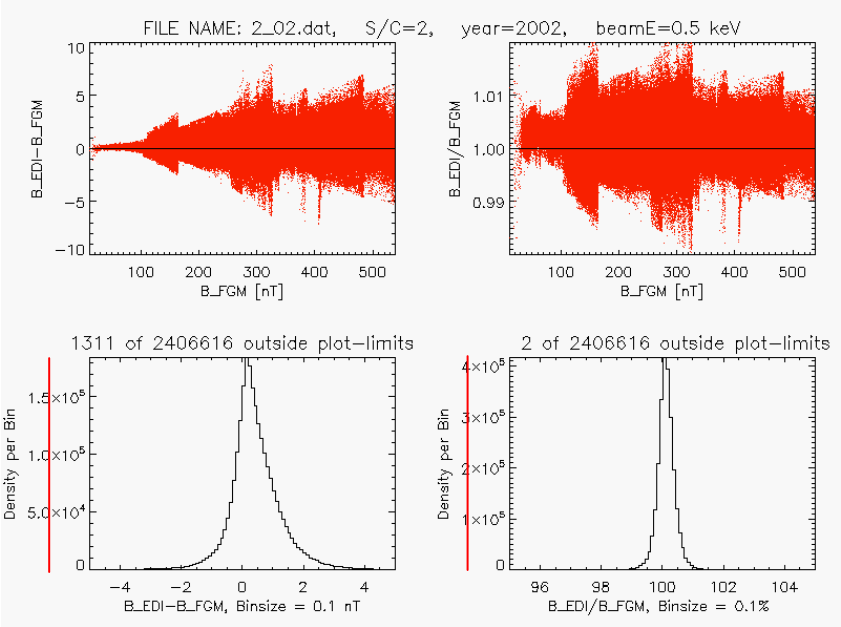

Figure 6.1 EGD Statistics for Cluster2, 33 orbits in 2002

A possible scaling error of the FGM data was considered, but not corrected, because of the big spread of the distribution and other possible sources of errors. A scaling factor correction would take care of both observed shift of the ratio distribution (see 3d Cross-Calibration meeting, 26-27 Oct 2006, MSSL, Dorking).

Other sources for the discrepancies were studied. One example is given below: Comparison of EDI and FGM using data from C3, 2003-08-02 (choosing the time domain) and investigating which improvements can be made. High resolution FGM data were produced using daily calibration files (that is, not the FGM data from the Active Archive)

6.1.1 Relativistic mass correction

Relativistic mass correction for converting B magnitude to gyro-time has an effect is 0.2% for 1keV and 0.1% for 500eV electrons

6.1.2 Time-of-flight offsets and remaining B spin axis offset

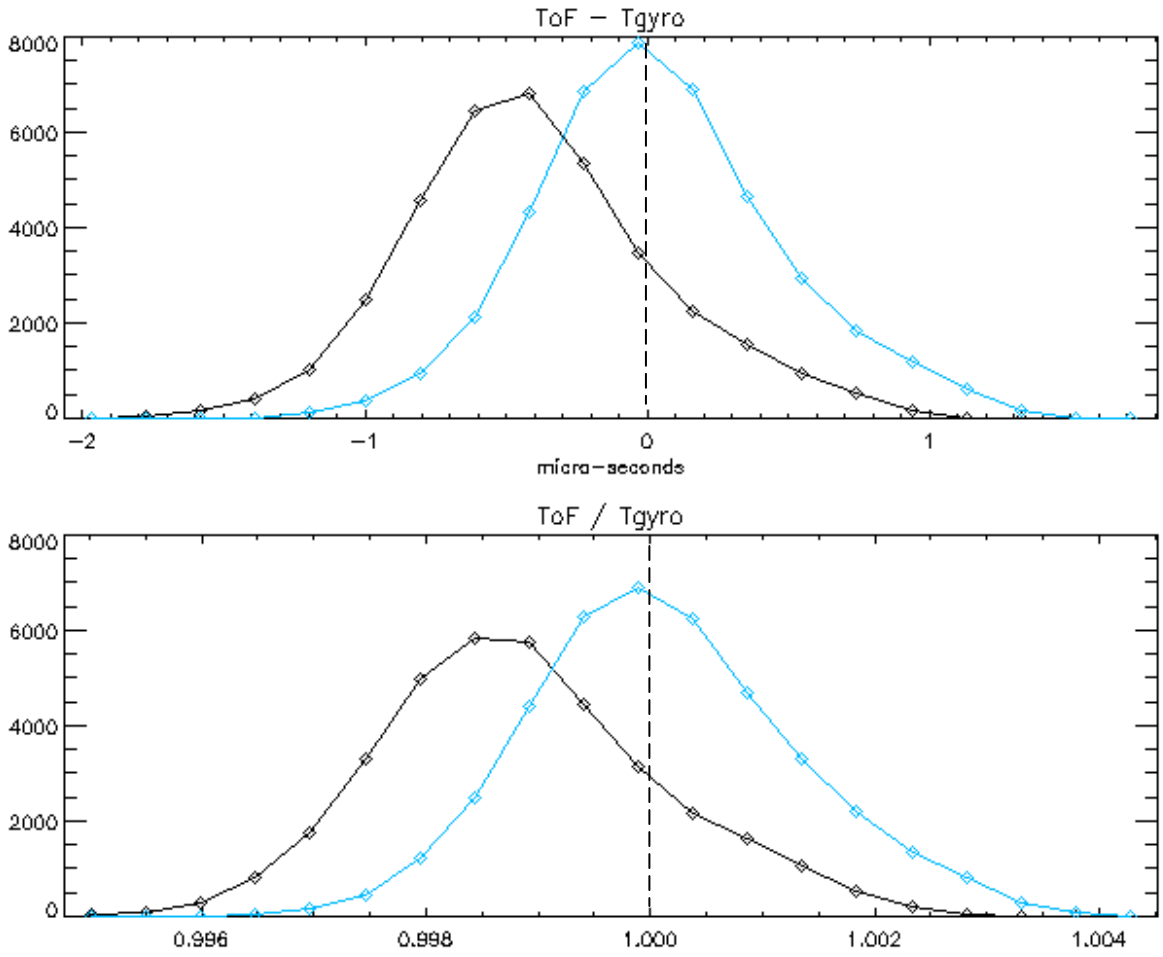

Figure 6.2 Distribution of the differences and ratios of EDI and FGM in time domain (gyrotimes)

A special IDL routine written by Hans Vaith was used to adjust for a given data set (that uses data from one FGM range and one EDI correlator chip frequency setting) the time-of-flight offsets and remaining spin axis offsets on B. The program was run on two subsets of the data from 2003-08-02. Both are FGM range 3, one with EDI short code the other with EDI long code. Using the offsets that are determined by this procedure (spin axis B offset between 0.1 and 0.2 nT, time-of-flight offsets of a little less than one micro-second) the match between times-of-flight and gyro-times improves (see the attached picture, where the black distribution is the uncorrected one and the blue distribution is the corrected one; the top panel shows ToF-Tgyro, the bottom panel shows ToF/Tgyro).

The problem with this procedure is that it cannot be run blindly (that is, automatically) on any dataset without manual quality control. The question here is, how good the calibration of B is?

6.1.3 Validity of "ToF1 + ToF2 = 2*Tgyro"

This question can be answered analytically by looking at the relation between the times-of-flight and the gyro-time, which is an implicit equation that can be solved by using Taylor series expansions and including terms of zero-th and first order. In

this approximation (first order) the above equation (ToF1 + ToF2 = 2*Tgyro) is derived. It turns out that this equation holds extremely well even when including higher orders. First of all, there are only contributions from odd-numbered orders in the Taylor series expansion (1st, 3rd, 5th, 7th etc). This means that the above equation actually holds to second order. When looking at higher order contributions it turns out that the major part of each contribution does not violate the above equation. For this reason deviations from this equation are so minor that they are beyond all interest (And they have a much smaller effect on results than for example the relativistic mass correction and the time-of-flight offsets and spin axis B offsets).

6.1.4 Averaging times-of-flight without separating into short (ToF1) and long (ToF2) times-of-flight

The currently employed procedure uses EDI EGD data and averages them over small time intervals for comparison to the gyro-times derived from FGM.

Strictly speaking this is valid only if the same number of short (ToF1) and long (ToF2) time-of-flight data points are present in the averaged time interval. In general this is not the case. For example, when the drift step is very small (high B, small E) only the short times-of-flight can be measured for geometrical reasons. However, in these cases the difference between time-of-flight and gyro-time is also small - a small fraction of a micro-second - , and therefore the error made by taking the average of the measured times-of-flight as a proxy of the gyro-time is smaller than effects caused by typical time-of-flight offsets and spin axis offsets of B.

The EGD dataset has the advantage that is can be used directly without requiring more advanced EDI analysis (drift step determination and separation of data points into short and long times-of-flight), at the expense of introducing errors that are smaller than the other error sources (offsets) and are - when sufficiently long time intervals are being used - negligible, unless B calibrations better than 0.1 to 0.2 nT are required.

6.2 EDI and WHISPER comparison

WHISPER is measuring high frequency wave spectra and can determine in certain conditions (plasmasphere) the gyro-frequencies of the electrons. This depends on the density of the electron and the visibility of the gyrofrequency and its harmonics in the spectrogram, since image processing methods are used. See Trotignon et al, 2008 contribution at the Cluster WS in Tenerife.

Cross-calibration of data delivered by three instruments (FGM, EDI, and WHISPER) was performed in the beginning in the magnetic field domain, but after observing a discrepancy between the fields deduced from WHISPER and EDI, the frequencies were compared directly. The comparison was done for 2001-2005.

Figure 6.3 shows the results for the years 2001-2003, spacecraft C1, C2, and C3 where EDI is working on. EDI data was averaged to the WHISPER acquisition time intervals. Red symbols show the average ratios of EDI over WHISPER electron gyrofrequencies per year and the blue ones are similar ratios for the magnetic field strength.

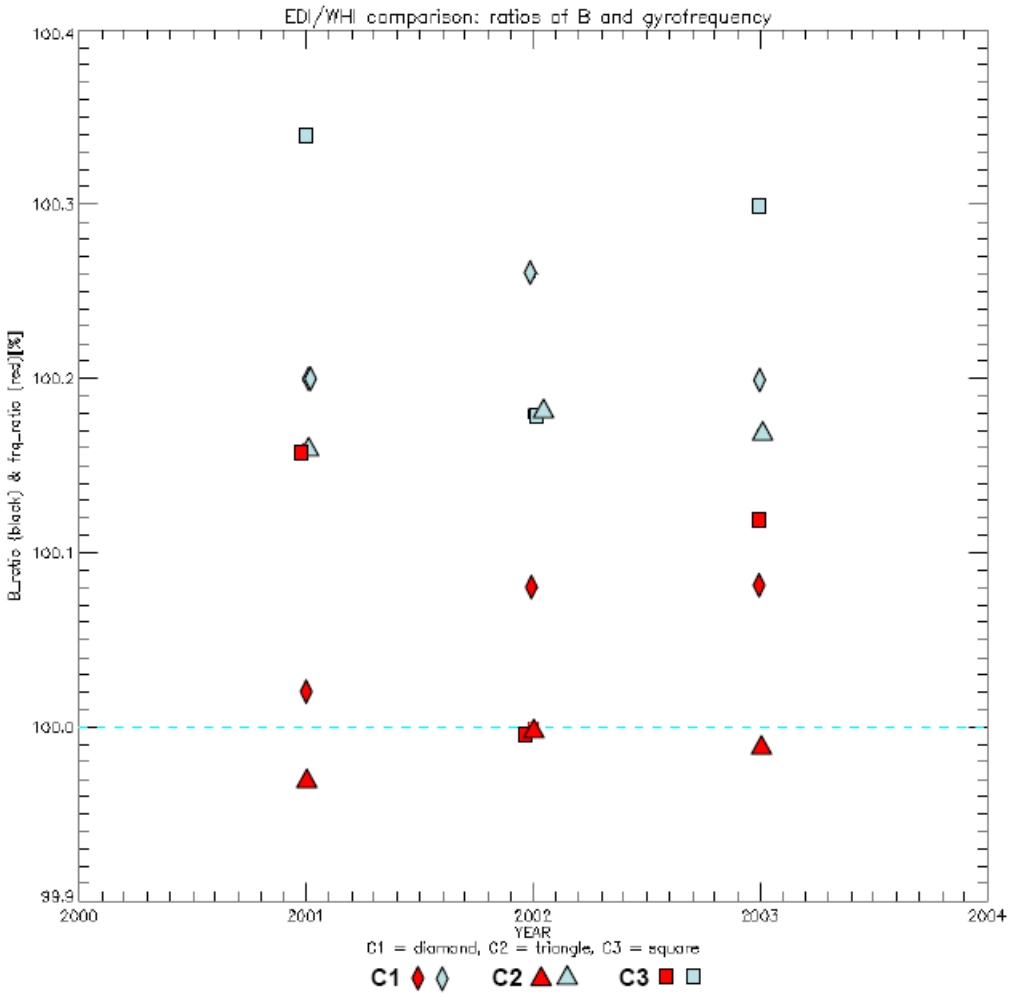

Figure 6.3 EDI/WHI ratios of electron gyrofrequencies (red) and magnetic field magnitudes (blue); the magnetic field magnitude ratio includes a relativistic correction for EDI.

The shift between the B and the time/frequency domain are due to the different coefficients used to convert the data. WHISPER didn't use a relativistic correction. There is no information about the energy of the electrons measured by WHISPER and why a relativistic correction should be appropriate.

Different coefficients used for conversion are responsible for the discrepancy. The comparison of WHISPER data for the last two years showed double peaked distribution both for comparison with FGM B and with EDI gyrofrequencies, which are probably also due to a mixture of cold and hot electron populations measured by WHISPER.

6.3 EDI and EFW electric field comparisons

The Cluster Electron Drift Instrument (EDI) and the Electric Fields and Waves experiment (EFW) both produce the electric field as one of their primary data products for the CAA. EDI measures the two perpendicular (to the magnetic field) components of the electric field. EFW measures the two electric field components in the spin-plane of the spacecraft. Under the assumption of negligible parallel electric field (i.e., the "E dot B = 0" assumption), the full perpendicular electric field can be constructed from the EFW spin-plane measurements, and direct EDI-EFW comparisons can be made.

Alternatively, EDI data can be rotated into the spacecraft coordinate system, and the spin-plane components can be directly compared to EFW. This has been done for comparison purposes in Figure 6.4, which shows Cluster 3 inner-magnetospheric data on 18-Mar-2002. From top to bottom are the X-component (sunward) and Y-component (duskward) of the electric field in DSI (despun-satellite-inverted) coordinates and in the spacecraft frame of reference, background 1 keV electron counts measured by EDI, and the absolute value of the spacecraft-to-probe potential measured by EFW. EDI is plotted in black and EFW in red. The co-rotation electric field is plotted in cyan. Large excursions from co-rotation at ~ 10:15 and 11:30 UT have been identified as subauroral ion drifts (SAID) (*Mishin and Puhl-Quinn* [5]). The spacecraft is in the polar cap at the beginning of the time series, and subsequent regions are indicated in Panel 3. Both the EDI and EFW electric field datasets plotted are CAA products: EDI PP-Plus data, and EFW L3 data.

The example in Figure 6.4 serves to illustrate two main points: 1) the EDI and EFW datasets are highly complementary and, 2) simultaneous EDI and EFW data provide valuable information regarding instrument performance. It is shown in Figure 6.4, and has been shown more extensively in *Puhl-Quinn et al*. [6], that one instrument's measurement difficulties in a particular region are often compensated for by measurement success by the other instrument. The dropout of EDI (black) data during the plasmasheet crossings in Figure 6.4 is due to high levels of background 1 keV electrons which interfere with the detection of the returning, coded electron beam emitted from the EDI electron gun. EFW, however, is measuring quite successfully the very large and fluctuating fields often encountered in this region. Both instruments detect the SAID fields. In the dense plasmasphere, however, only EDI is able to measure the small fields which approach co-rotation values. The EFW sunward component is erroneously offset from the EDI result. The EFW experiment suffers from saturation issues for the P34 probe pair (which is related to sub-optimal bias current settings for this region) and also from a non-sinusoidal P12 probe pair signal, which could be due to a small, cold plasma wake [Y. Khotyaintsev, private communication]. These types of problems are thought to be rather common in this dense region, and efforts to automatically exclude this type of EFW data from the CAA have been undertaken [*Khotyaintsev et al.*, 7th CAA Cross-Calibration Meeting, Tenerife, 2008].

Event analyses such as this one are ongoing, in an attempt to produce a merged EDI/EFW dataset in the inner magnetosphere which is larger than either dataset alone, due to the high degree of complementarity existing between them, and which is composed of the highest quality data possible. A preliminary version of a merged dataset using only Cluster 1 data, from 2001-2003, is described in *Puhl-Quinn et al.* [5]. With the recent reprocessing and redelivery of the EFW CAA data for the years 2001-2005, our efforts can continue, and a new version of the merged dataset using all spacecraft from 2001-2005 is currently under development.

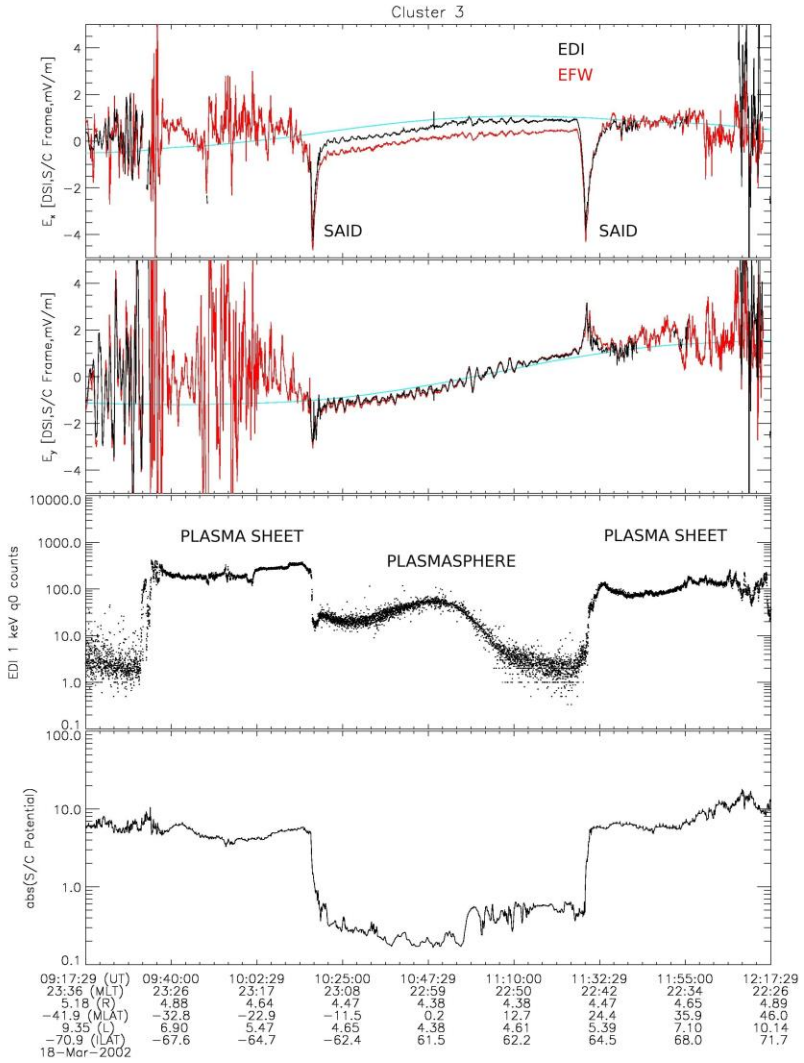

Figure 6.4. EDI and EFW electric field comparison in the inner magnetosphere. Cluster 3 data is plotted from 18-Mar-2002. From top to bottom are the X-component (sunward) and Y-component (duskward) of the electric field in DSI (despun-satellite-inverted) coordinates and in the spacecraft frame of reference, background 1 keV electron counts measured by EDI, and the absolute value of the spacecraft-to-probe potential measured by EFW. EDI is plotted in black and EFW in red. The co-rotation electric field is plotted in cyan.

6.4 EDI Ambient Electron Data Comparison to PEACE

It is natural to compare the EDI AE data with the PEACE electron observations. PEACE measures electrons in an energy range between 0.7 eV and about 30 keV and at all pitch angles with one spin resolution (~4 s). Figure 6.5 below compares EDI AEDC and PEACE data in the parallel direction obtained by SC 2 between 0600 and 0630 UT, 5 June 2002, when the spacecraft was located at the dawnside magnetosphere measuring precipitations of magnetosheath-like electrons.

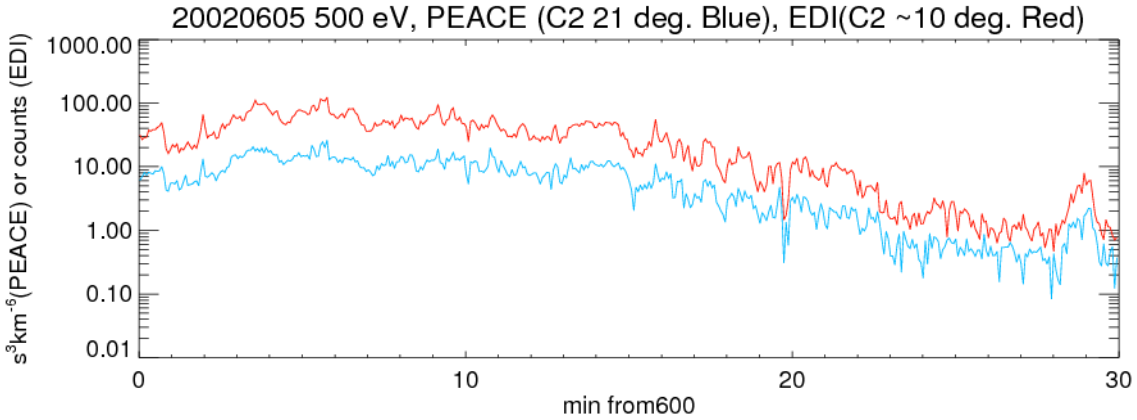

Figure 6.5. Comparison between PEACE distribution function and EDI AEDC counts at 500 eV between 0600-0630 UT on 5 June 2002. Data close to parallel pitch angles are presented.[6]

The EDI AEDC data are averaged to 4 s resolution to yield better comparison with PEACE data. As time proceeds, both the electron counts and phase space density gradually decrease by two orders of magnitudes from initial values. Also, EDI data (red) and PEACE data (blue) show a similar small-scale variation. The correlation coefficient between these two quantities is quite high, indicating their ratio is rather constant. This result is similar when we choose data from other pitch angles. It would be possible to convert EDI's counts to the physical quantities such as phase space density or flux by multiplying by a factor derived from this type of comparison. Although the ratio seems to be constant during 30 min of one day, this value is variable on a monthly and yearly basis, possibly caused by degradation of the detectors. It should be noted that the design of the detector part of EDI is not optimized to measure natural electron counts since the original purpose is to measure artificial electron beams from which it is possible to derive E×B drift or electric field. So far, the EDI-PEACE cross-calibration has not been performed for recent data, except on a case-by-case basis.

For calibration purpose we have used the PEACE data product: spin resolution differential energy flux (C2_CP_PEA_PITCH_SPIN_DEFlux__20051022_0850_1140_V01.cef in our example). The differential energy fluxes were selected for pitch angles [°]: 7.5 (0), 172.5 (180) and 82.5, 97.5 (90) and energies [keV]: 0.5399 (0.5) and 1045.10 (1.0). In this case the energy was 1 keV for AE as most of the time; the energy of 0.5 keV is used rarely.

EDI corrected counts (**corrected_count2**) were averaged to the PEACE time-intervals. The calibrated counts were obtained by multiplying with the calibration factor determined by

cal_count = corrected_count2*f_cal

f_cal = <flux_PEA>/< **corrected_count2**>, averaging was made over the whole time interval.

Figure 6.6 shows the high resolution calibrated counts (**cal_count**) for both detectors (blue and black) and the averaged values (no distinction between detectors made) to the PEACE times (green), the red squares show the spin resolution PEACE fluxes. A constant calibration factor was used.

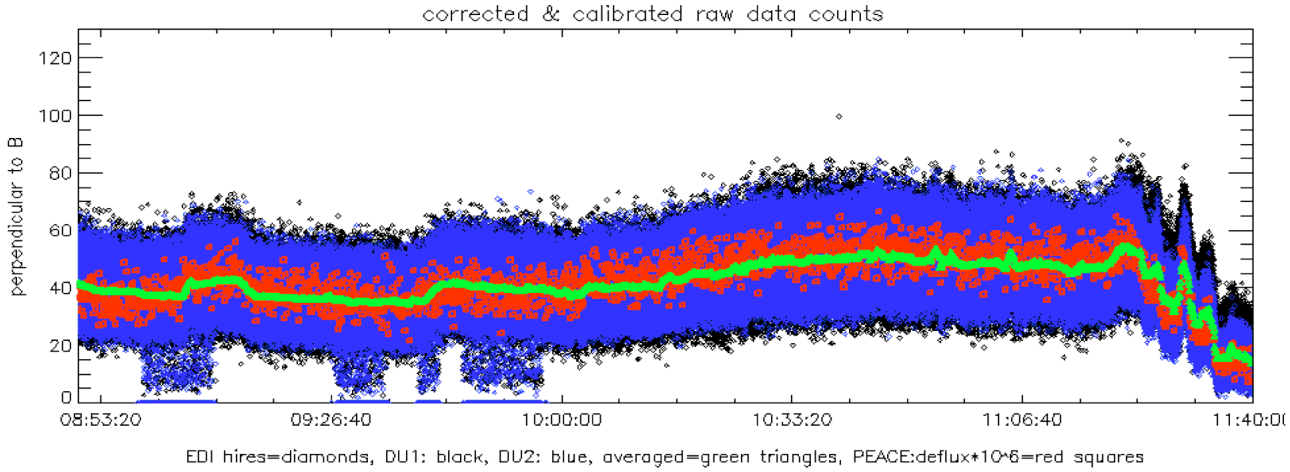

Figure 6.6. Corrected and calibrated ambient electron counts with pitch angle 90°. GDU1: black and GDU2: blue. PEACE differential electron fluxes: red squares, Green triangles are the averages of the AEDC data for the PEACE acquisition time intervals.

The agreement is good except for the last 20 minutes, where the assumption of "constant" inter-detector correction factor fails (see left panel of Fig 6.7 and the shift between the blue and black data points). The EDI data are smoother than PEACE data when averaged down to spin frequency, but the high resolution data have a much larger spread, so in order to have electron data with a higher than spin resolution one has to average the data.

Figure 6.7 shows variations of the correction and calibration factors for ~3 hours of data. The black lines are the "high resolution" factors and the colour ones spin averages. The dark blue (left) and red (right) horizontal lines are the constant factors used for correction and calibration. The light blue and green curves in the left panel show the difference between averaging the high resolution **f_id** (in black) and calculating the ratios of averaged data.

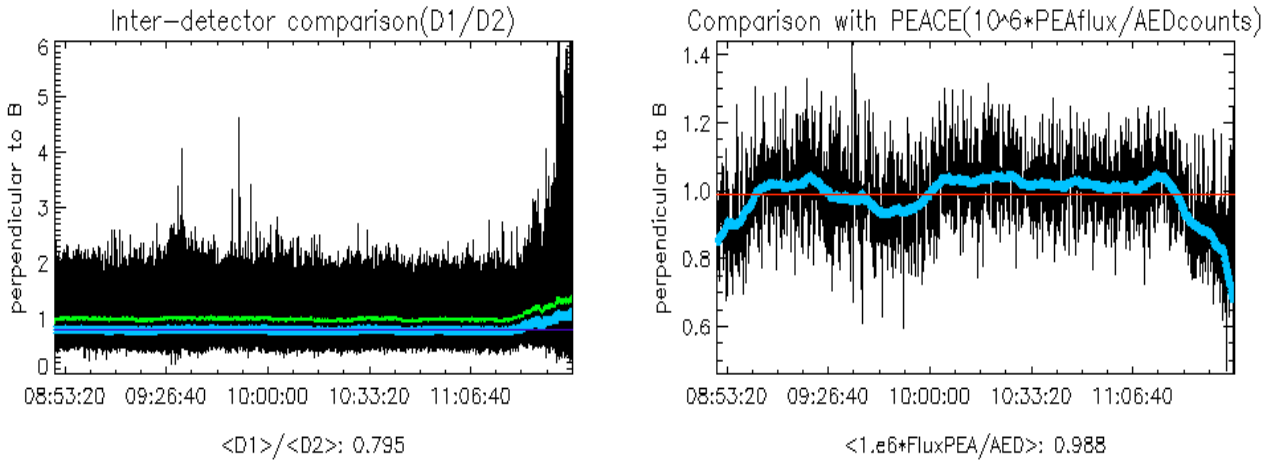

Figure 6.7. Inter-detector (**f_id** – left panel) and calibration (**f_cal*10^6** – right panel) factors for 22 October 2005, 08:50-11:40 UT. High resolution factors (thin black), averages over the PEACE acquisition time intervals ~4s (thick light blue) and medians of the factors for the same intervals (green line). The thin blue line in the left panel and the red line on the right are the mean values for the whole time interval.

A large-scale effort to compare large amounts of EDI AE data to PEACE would be necessary in the future in order to quantify the EDI counts and to understand the characteristics of the sensitivity of the detector on EDI. Users are encouraged to contribute to this effort by using the procedure exemplified below for AE correction and calibration.

DIFFICULTIES / CAVEATS:

- Energies and pitch angles not exactly the same
- The different factors (**f_id, f_cal**) are not constant in time, see Figure 6.7
- The determination of the factors is a time-consuming process
- The factors/errors depend on the selected averaging intervals and are not well defined

7 Summary

The four cross-calibration activities EDI is involved in will continue for newer data sets as far as time is available.

- The discrepancies between the EDI, FGM and WHISPER magnetic field magnitude data used in these comparisons are within 0.4%.
- The discrepancy in frequency between EDI and WHISPER is within 0.1%; no explanation is found for this agreement, since EDI electrons need relativistic mass correction and the WHISPER ones probably not.
- EDI and EFW electric field data complement each other and should be used together
- For the AE calibration a large effort is needed to produce the inter-detector correction files and to make systematic comparisons to PEACE. The procedure is described and the EDI team offers assistance to any users willing to participate.

8 References

[1] EDI ICD http://caa.estec.esa.int/caa/ug_cr_icd.xml

[2] Paschmann G. et al., *The Electron Drift Instrument on Cluster: overview of first results*, Annales Geophysicae (2001) 19: 1273–1288

[3] Quinn, J. M., *Cluster EDI convection measurements across the high-latitude plasma sheet boundary at midnight*, Annales Geophysicae (2001) 19: 1669–1681

[4] Georgescu, E., H. Vaith, K-H. Fornacon, U. Auster, A. Balogh, C. Carr, M. Chutter, M. Dunlop, M. Foerster, K-H. Glassmeier, J. Gloag, G. Paschmann, J. Quinn and R.Torbert, *Use of EDI time-of-flight data for FGM calibration check on CLUSTER*, Proceedings of the Cluster and Double Star Symposium 5th Anniversary of Cluster in Space, ESA SP 598, P6.9, (2006)

[5] Mishin, E. V. and P. A. Puhl-Quinn (2007), SAID: *Plasmaspheric short-circuit of substorm injections*, Geophys. Res. Lett., Vol. 34, L24101, doi: 10.1029/2007LG031925.

[6] Puhl-Quinn, P. A., H. Matsui, V. K. Jordanova, Y. Khotyaintsev, and P.-A. Lindqvist, *An effort to derive a convection electric field model in the inner-magnetosphere: Merging Cluster EDI and EFW data*, Journal of Atmospheric and Solar-Terrestrial Physics/ (2007), doi:10.1016/j.jastp.2007.08.069

[7] Kogler, C., *Boundary Detection in Space Plasmas within ESA's Cluster II Mission*, Master Thesis, IWF, TU Graz, http://www.student.tugraz.at/christian.kogler/EDI/thesis.pdf, 2009

[8] Paschmann G. et al., *The Electron Drift Instrument for CLUSTER,* Space Science Reviews, Volume 79, Numbers 1-2, Pages 233-269, 1997